Journal of Materials Chemistry A

Local structure heterogeneity in unique tetragonal BaTiO3-based relaxor featuring ultrahigh electrostrictive effect

Journal:	*Journal of Materials Chemistry A*
Manuscript ID	TA-ART-08-2023-004557.R1
Article Type:	Paper
Date Submitted by the Author:	12-Sep-2023
Complete List of Authors:	Yao, Yonghao; University of Science and Technology Beijing Wang, Lu; University of Science and Technology Beijing Zhang, Yuanpeng; Oak Ridge National Laboratory Liu, Jue; Oak Ridge National Laboratory, Chemical and engineering Materials Huo, Chuanrui; University of Science and Technology Beijing Liu, Hui; University of Science and Technology Beijing Chen, Jun; University of Science and Technology Beijing, Department of Physical Chemistry; Hainan University

ARTICLE Journal Name

Local structure heterogeneity in unique tetragonal $BaTiO_3$-based relaxor featuring ultrahigh electrostrictive effect

Received 00th January 20xx,
Accepted 00th January 20xx

DOI: 10.1039/x0xx00000x

Yonghao Yao, [a] Lu Wang, [a] Yuanpeng Zhang, [b] Jue Liu, [b] Chuanrui Huo, [a] Hui Liu*[a] and Jun Chen*[a,c]

Relaxor ferroelectrics are characterized by nanoscale structural heterogeneity and show superior electrical properties. However, the complicated local structures are not well deciphered in lead-free counterparts and impeding the understanding of structure-properties relationship. Herein, the temperature-dependent local structures of unique tetragonal $BaTiO_3$-$(Bi_{0.5}Li_{0.5})TiO_3$ relaxor which present an ultrahigh electrostrictive effect, are studied by using the neutron total scattering. Significant tetragonal distortion at 1-10 Å local scale persists between 100-500 K, despite the long-range structure having undergone a tetragonal to cubic phase transition. Interestingly, nanoscale Li-Bi clusters exist in the Ba matrix, which hold large polar displacements and remain even above T_m. A gradual disorder in the local polarization direction with an increase in temperature, accompanied by a nearly constant spontaneous polarization magnitude. This phenomenon leads to the vanishing of macroscopic polarization during the diffuse phase transition. These findings contribute to a better understanding of the role of local chemical heterogeneity on the relaxor behavior, and provide a structural foundation for designing relaxors by utilizing short-range chemical ordering.

Introduction

Relaxor ferroelectrics (RFEs) are featured as strong frequency dispersion of dielectric permittivity, frequency-dependent dielectric maximum (T_m), and diffused phase transition (DPT), making them highly attractive for a wide range of applications in sensing, transduction, and energy storage.[1-10] The fascinating properties of RFEs are thought to be linked with the heterogeneous polar structures.[11-17] Initially, RFEs were treated with models based on the compositional fluctuation that deviating from the completely disorder solid solutions.[18-21] The widely accepted theory for explaining the dielectric anomaly is rooted in the local polarization correlations at the nanoscale, known as polar nanoregions (PNRs). Various models have been proposed to rationalize the complicated polar structures, such as chemical order/disorder, random electric fields, low angle domain walls, and dipolar glasses.[11,12,22,23] While most of these developed models are formed on the lead-based relaxor systems, such as $Pb(Mg_{1/3}Nb_{2/3})O_3$ (PMN), $Pb(Sc_{1/2}Nb_{1/2})O_3$ (PSN) and $Pb(Zn_{1/3}Nb_{2/3})O_3$ (PZN). Notably, all these lead-based materials present a DPT from long-range rhombohedral (*R*) to cubic (*C*) symmetry. Thus, some adaptations may be required to apply these models to lead-free counterparts.

Over decades, numerous lead-free relaxors with diverse chemical compositions and structures have been developed,[3,4,6,8,24-26] which provide exotic specimens for understanding the physics behind relaxor behaviours. Very recently, a giant electrostrictive effective has been reported in $BaTiO_3$-$Bi_{0.5}Li_{0.5}TiO_3$ (BT-BLT) relaxor, where A-site consists of small radius Li^+, covalency Bi^{3+}, and large pure ionic Ba^{2+}.[26] Interestingly, the BT-BLT solid solutions exhibit the tetragonal (*T*) phase at low temperatures, in contrast to the common R-phase shown in lead-based counterparts, such as PMN. Hence, exploring the detailed local chemistry and local structure across the DPT in the unique tetragonal lead-free relaxor would enhance the understanding of the relaxor behaviours.

The atomic pair distribution function (PDF) based on total scattering techniques has garnered increasing attention due to its ability to capture short-range local and long-range average structures simultaneously in complex functional materials.[27,28] PDF enables to detect the structural information, including bond lengths and coordination surroundings in real space. For instance, the use of this technique has unveiled local polar states that are distinct from the long-range average structures.[29,31] Further, combined with the big box modelling method reverse Monte Carlo (RMC) algorithm,[32] the A/B-site position and displacement distribution can be obtained in perovskites.[15,29,33]

Herein, we report the evolution of local structures in a unique tetragonal $0.85BaTiO_3$-$0.15Bi_{0.5}Li_{0.5}TiO_3$ (BT-15BLT) relaxor. The *T* distortions at different scales are revealed by X-ray diffraction and neutron total-scattering. The short-range structure maintains abnormal *T* distortion while the macroscopic phase structure has transformed from *T* ferroelectric to paraelectric phase. By combining the RMC simulations, we show that the clusters can result in structural distortion and PNRs. The origin of relaxation transition is certified to polarization rotation from the atomic distribution configuration. This study enhances the comprehension of polarization distribution configurations in relaxors and provides novel insights for their design.

Results and discussion

The BT-100*x*BLT ($0.1 \le x \le 0.17$) was prepared by solid-state reaction method. With increasing BLT content, the solid solution transforms from a typical ferroelectric state to a RFE state according to the *P-E* loop and dielectric spectrum (Fig. S1(a)). Particularly, the almost zero remanent polarization indicates that typical RFE state has been obtained at $x = 0.15$. As reported in our previous study,[26] the BT-15BLT present

[a] Beijing Advanced Innovation Center for Materials Genome Engineering, Department of Physical Chemistry, University of Science and Technology Beijing, Beijing 100083, China.
[b] Chemical and Engineering Materials Division, Oak Ridge National Laboratory, Oak Ridge, Tennessee 37831, USA.
[c] Hainan University, Haikou 570228, Hainan Province, China
Electronic Supplementary Information (ESI) available: [details of any supplementary information available should be included here]. See DOI: 10.1039/x0xx00000x

hysteresis-free polarization-strain (Fig. 1). This lead to an ultrahigh electrostrictive effect with Q_{33} of ~0.0712 m^4/C^2. In contrast to the obvious phase transition of R-O and T-O in $BaTiO_3$ (BT),[34] no ferroelectric phase transition is observed in the BT-100*x*BLT system (Fig. S1(b)). The BT-15BLT shows strong diffuse phase transition and board frequency dispersion of T_m as shown in Fig. 1(a). ΔT_m reaches about 100 K with the frequency varying from 1 kHz to 1MHz accompanied with a relaxation parameter γ of 1.63 (Fig. S1(c)). These behaviours are similar to conventional lead-based relaxors and $Ba(Ti,Zr)O_3$ relaxors.[12,35] However, the ultrahigh electrostrictive effect imply the local polarization feature would be different.

The long-range average structure of BT-15BLT is studied by the X-ray diffraction (XRD). Interestingly, the BT-15BLT presents long-range *T* phase at low temperature. It is known that the BT shows *R* phase at low temperature. Therefore, most of $BaTiO_3$-based relaxors exhibits long-range *R* symmetry at low temperature.[34,36] It seems that the *T* phase relaxors is rare both in lead-based and lead-free-based relaxors. From the 125 - 475 K, only long-range ferroelectric *T* to *C* phase transition around 300 K is detected (Fig. 2(a)), which is consistent with the dielectric spectrum (Fig. 1). The temperature dependent structure parameters are presented in Fig. 2(b). The long-range *T* distortion is approximately 1.007 at 125 K, and gradually decreases to 1 at around 325 K. Of particular interest is probing the evolution of local structure under the unique long-range *T* to *C* DPT in BT-15BLT relaxor.

The neutron total scattering is employed to study the local structures of BT-15BLT. Fig. 3(a) displays the PDF within the range of 1.5 - 4.5 Å, revealing the nearest coordination information of perovskite structures. No abrupt change in the PDFs is observed from 100 K and 500 K, which differs from the results obtained from XRD. The peaks at roughly 1.8 Å correspond to Ti-O pairs, while the peaks between 2.3 - 3.2 Å represent *A*-O and O-O pairs. The presence of peak asymmetry in Ti-O and *A*-O peaks across the entire temperature range suggests the occurrence of local off-central displacements from their surrounding oxygen cages. PDF fitting under different length scales reveals a significant local *T* distortion of 1.014 below 10 Å (Fig. 3(b) and Fig. S2), which persists even when the temperature exceeds T_m (Fig. 3(c)). At medium-length scales (< 40 Å), the variation trend of *c*/*a* with respect to temperature derived from the long-range PDF results is consistent with the refinement results collected from XRD refinement. The disparity in *T* distortion primarily manifests during DPT, as observed from the refinement results obtained from neutron total scattering and XRD. Thus, the presence of deviation between the short-range local structure and long-range average structure is deemed to be an essential feature of DPT in relaxors.

The big-box modelling based on RMC method enables to effective analyse the spatial variation of local atomic distribution, which plays a critical role in understanding the relaxation characteristics of RFEs that are strongly related to compositional heterogeneity.[15] A big 3D model with approximately 80 Å × 80 Å × 80 Å is adopted to refine the PDF *G*(*r*) and *S*(*Q*) data simultaneously. Both the structural signatures in very local and long-range from real-space and reciprocal space can be restored (Fig. 4(a)). Note that *A*-site atoms are allowed to swap randomly during RMC simulations,[32] and thus can get the atomic spatial distribution information. Interestingly, evident nanoscale inhomogeneous chemical distribution is observed. Li and Bi aggregations embedded into the Ba matrix occur with several unit-cell sizes (Figs. 4b and 4c). Notably, these chemical clusters formed by the Li and Bi aggregations persist throughout the temperature range of 100 - 500 K (Fig. S3). It appears that the clusters are not significantly affected by temperature. Currently, there is a growing consensus that lead-based PMN RFEs demonstrate a well-defined ordering of Mg/Nb at the nanoscale, with non-random cluster arrangements.[14] In contrast, the Li-Bi clusters of BT-15BLT display a disordered distribution within the nanoscale clusters, showing no apparent correlation between clusters within the supercell.

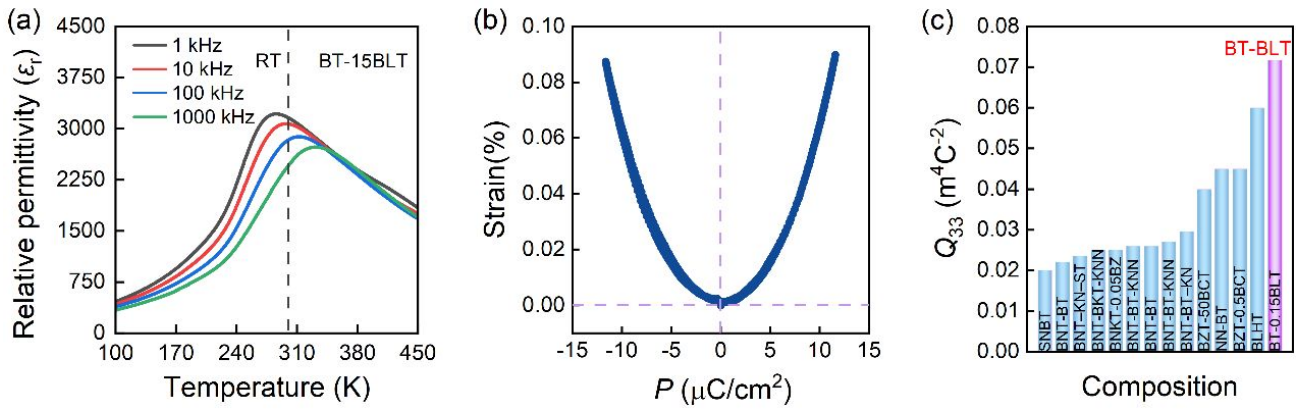

Fig. 1 (a) Temperature-dependent permittivity, and (b) strain-polarization curve of BT-15BLT ceramic at room temperature. (c) Comparison of Q_{33} value in representative lead-free ceramics.

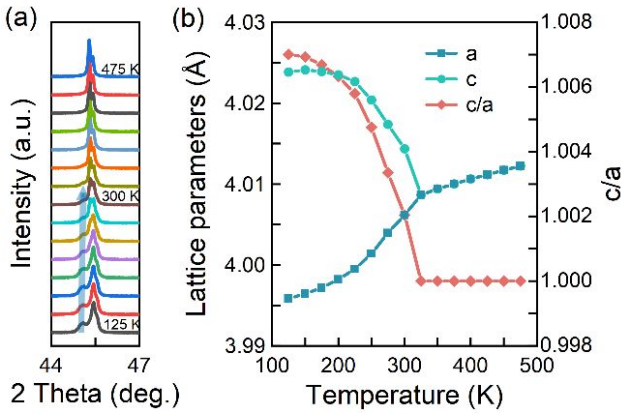

Fig. 2 (a) Temperature-dependence (002) peak, and (b) lattice parameters from the refine structure at different temperature of BT-15BLT.

The complex polar structure of relaxor is closely related to the local chemical heterogeneity.[12,13,20] Therefore, the atom polar displacement and unit-cell polarization are extracted to elaborate the relationship between chemical clusters and PNRs. Fig. 4d illustrates the calculated 3D distribution of *A*/*B*-site polar displacements. As depicted, the displacement clusters associated with *A*-site atoms exhibit smaller volumes compared to those generated by *B*-site atoms, consistent with the size of the Bi-Li clusters shown in Fig. 4c. The Ba matrix associated with *A*-site atoms shows negligible polarization displacement, indicating a higher degree of Ti-O hybridization compared to Ba-O. This finding aligns with the well-established understanding that the ferroelectric polarization in $BaTiO_3$ is primarily induced by *B*-site atoms. Notably, the displacement magnitude generated by *A*-site atoms surpasses that of *B*-site atoms, implying that the introduction of Bi/Li atoms triggers higher polarization at the *A*-site. Intriguingly, both *A*-site and *B*-site displacement clusters exhibit corresponding polarization clusters. These polarization clusters, also referred to as PNRs, interrupt the long-range ferroelectric polarization alignment. Significant polarization displacement differences and non-uniform distribution within these clusters provide a strong restoring force for polarization reversal. Furthermore, the substantial atomic polar displacements of Bi and Li induce a robust strain response, resulting in a large hysteretic-free strain that ultimately yields an ultrahigh electrostrictive effect with Q_{33} of ~0.0712 m^4/C^2. However, the contributions of *A*-site and *B*-site displacements to the spontaneous polarization need to be considered in terms of overall averaging results.

The evolution of mean atom polar displacement and unit-cell polarization with temperature is shown in Fig. 5. One can see that the length of Ti polar displacement is larger than *A*-site polar displacement. Because, the *A*-site is primarily occupied by pure ion-type Ba, while the *B*-site Ti can form covalent bonds with O. The local Ti polar displacement remains consistent at approximately 0.19 Å, and is not affected by changes in temperature. Conversely, the local *A*-site polar displacement increases with temperature. This phenomenon is likely due to the increased unit cell volume providing more displacement space for the small-radius Li^+ and Bi^{3+} ions as the temperature increases. Additionally, the polar displacement may be influenced by contributions from atomic thermal vibrations. Although the *A*-site polar displacement gradually reaches 0.18 Å, the Ti polar displacement still exceeds that of the *A*-site. This suggests that the macroscopic ferroelectric polarization of BT-15BLT is primarily driven by the *B*-site. By considering the synergistic contribution of both *A*-site and *B*-site, the local unit-

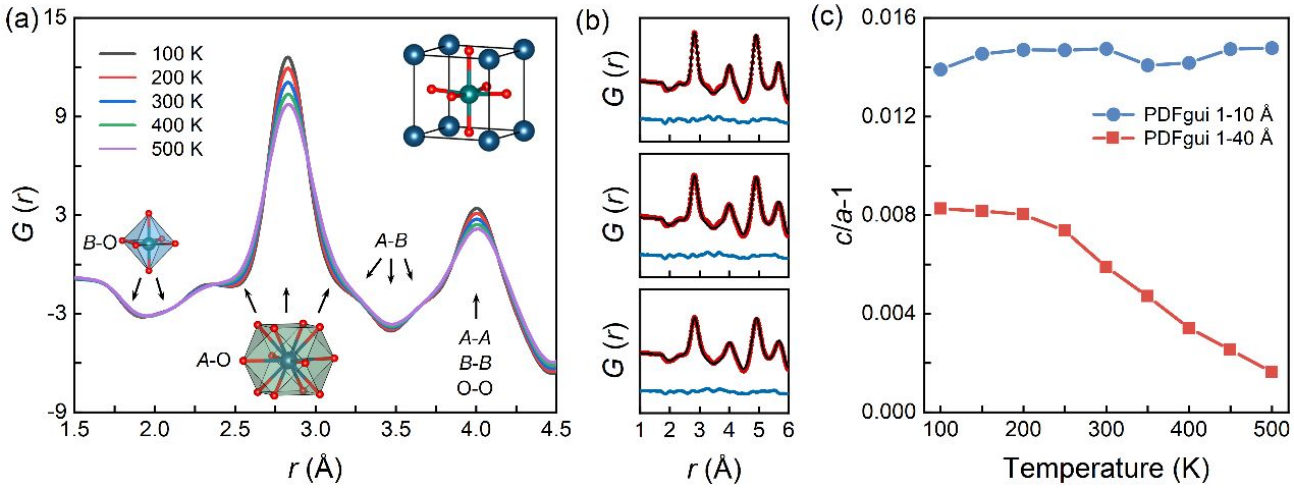

Fig. 3 (a) Selected PDF *G*(*r*) from 1.5 - 4.5 Å varying with temperature. (b) Short-range PDF fitting at 100 K, 300 K, and 500 K are shown from top to bottom. Red points, black lines, and blue lines indicate the experiment data, calculated data, and residual curves, respectively. (c) Temperature evolution of tetragonal distortion under different scales.

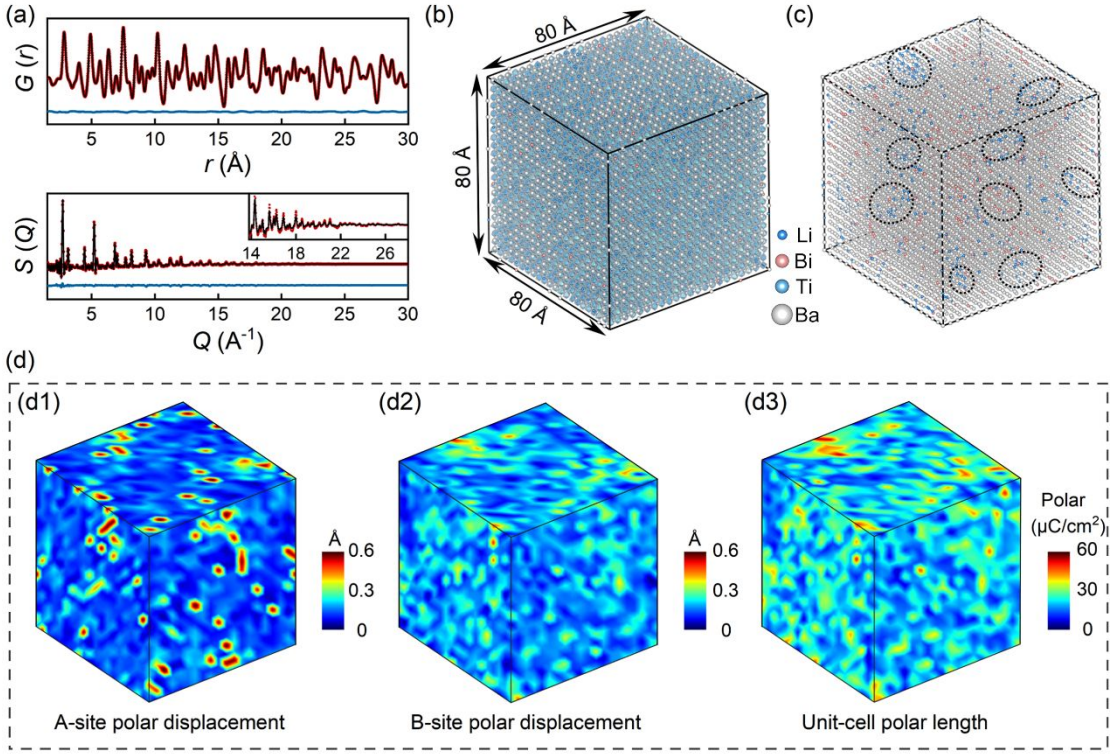

Fig. 4 (a) Experiment data (red points), calculated data (black lines), and residual curves (blue lines) of $G(r)$, $S(Q)$ using RMC simulation. (b) 3D atomic configuration with about 80 Å × 80 Å × 80 Å refined supercell. (c) A-site atoms 3D distribution in the refined supercell. (d) 3D distribution of A/B-site polar displacements and unit-cell polar length, corresponding the 3D atomic configuration of (b). All the data shown in this figure were obtained at 300 K.

cell polarization shows a slightly decreasing trend with increasing temperature. However, even at a temperature of 500 K, the local unit-cell polarization exists, with a value of 15.4 μC/cm². These observations agree with the persistent local *T* distortion. Notably, the macroscopic polarization gradually disappears during DPT. Therefore, it is not possible to fully understand this behaviour based solely on the length of local atomic polar displacement.

In addition to the magnitude of the unit-cell polar vector, the distribution of polar vector directions is crucial for determining the ferroelectric properties. Therefore, the evolution of polarization direction is analysed by examining the polar graph projections (Fig. 6). At 100 K, the polarization distribution of BT-15BLT exhibits similarities to the pure BT RMC results at room temperature, with a much more diffusion.[25] This indicates that the introduction of Bi and Li atoms contributes to the diversity of polarization directions. However, the polarization direction is predominantly aligned along the $[001]_c$ direction. As the temperature increases, the polarization viewed along $[100]_c$ of the BT-15BLT relaxor rapidly transitions towards disorder. Around the T_m temperature (300 K), the polarization along the *c* axis transforms randomly into arbitrary directions. Furthermore, the regions (blue region) of low polarization density occurs a further reduction. This phenomenon is observed in the distribution of polarization within the ab plane as well. Notably, the polarization distribution tends to be disordered at room temperature corresponding to the DPT. In the variable-temperature ferroelectric test, the macroscopic P_{max} gradually decreases from 12 μC/cm² at 300 K to 6 μC/cm² at 425 K (Fig. S4, and Fig. S5). However, the mean of unit-cell polar length remains 15.4 μC/cm², this discrepancy could be attributed to the cancellation

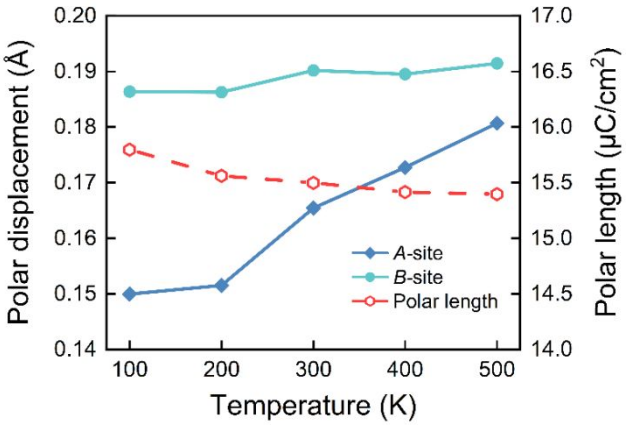

Fig. 5 Mean A-site and B-site polar displacement and unit-cell polar length with respect to temperature.

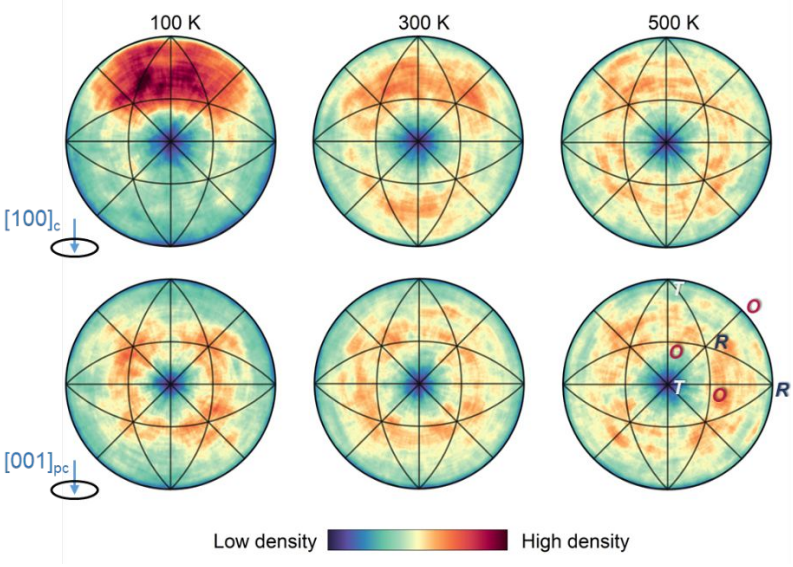

Fig. 6 Stereographic projection of unit-cell polar vector directions extracted from the refined atom configuration, viewed along $[001]_c$, $[100]_c$, at 100 K, 300 K and 500 K, respectively.

of disordered polarization arrangements, resulting in the disappearance of macroscopic polarization while local polarization remains. Consequently, the origin of DPT is certified to polarization rotation from the atomic distribution configuration. The polarization rotation behaviour could be attributed to the thermal activation process.[37] At the low temperature of 100 K, the local polarization is frozen to be distributed near the energy-favourable state, in which the polarization direction tends to *c* axis in BT-15BLT ceramics. When the temperature has exceeded enough, local displacement could rotate to a random orientation by thermal activation. Moreover, the atomic displacement is more diffusive resulting from the significant thermal vibration at higher temperatures. The disordered degree of the spontaneous polarization distribution increases in the polar graph projection. Hence, the polarization rotation combines the local structure with the average structure in RFEs, which provides profound DPT understanding and routes for designing RFEs.

Conclusions

In summary, the local structural features of the unique tetragonal BT-15BLT relaxor are elucidated by neutron total scattering combined with big-box RMC modelling. Within the temperature range of 100-500 K, tetragonal distortion remains at the scale of 2-3 unit cells while the macroscopic phase transition from tetragonal to cubic occurs. It is found that the Bi-Li clusters occurs within the Ba-matrix, leading to component disorder, and forming PNRs that correlated with significant polarization. The disruptive effect of the disordered local polarization results in the loss of macroscopic polarization near T_m. Essentially, the DPT is induced by polarization rotation. These findings enhance our understanding of the local structural evolution of relaxors.

Conflicts of interest

There are no conflicts to declare.

Acknowledgements

This work was supported by the National Natural Science Foundation of China (Grant Nos. 22075014, and 22235002). A portion of this research used resources at the Spallation Neutron Source, a DOE Office of Science User Facility operated by the Oak Ridge National Laboratory. The high-resolution synchrotron X-ray diffraction patterns were collected on the BL02B2 beamline of SPring-8 with the approval of the Japan Synchrotron Radiation Research Institute.

References

1 F. Li, M. J. Cabral, B. Xu, Z. Cheng, E. C. Dickey, J. M. LeBeau, J. Wang, J. Luo, S. Taylor, W. Hackenberger, L. Bellaiche, Z. Xu, L. Q. Chen, T. R. Shrout and S. Zhang, *Science*, 2019, **364**, 264-268.

2 S. Zhang, F. Li, X. Jiang, J. Kim, J. Luo and X. Geng, *Prog. Mater. Sci.*, 2015, **68**, 1-66.

3 A. R. Jayakrishnan, J. P. B. Silva, K. Kamakshi, D. Dastan, V. Annapureddy, M. Pereira and K. C. Sekhar, *Prog. Mater. Sci.*, 2023, **132**, 101046.

4 H. Pan, S. Lan, S. Xu, Q. Zhang, H. Yao, Y. Liu, F. Meng, E. J. Guo, L. Gu, D. Yi, X. Renshaw Wang, H. Huang, J. L. MacManus-

Driscoll, L. Q. Chen, K. J. Jin, C. W. Nan and Y. H. Lin, *Science*, 2021, **374**, 100-104.
5 H. Liu, Z. Sun, J. Zhang, H. Luo, Q. Zhang, Y. Yao, S. Deng, H. Qi, J. Liu, L. Gallington, J. Neuefeind and J. Chen, *J. Am. Chem. Soc.*, 2023, **145**, 11764-11772.
6 J. Yin, X. Shi, H. Tao, Z. Tan, X. Lv, X. Ding, J. Sun, Y. Zhang, X. Zhang, K. Yao, J. Zhu, H. Huang, H. Wu, S. Zhang and J. Wu, *Nat. Commun.*, 2022, **13**, 6333.
7 H. Tao, H. Wu, Y. Liu, Y. Zhang, J. Wu, F. Li, X. Lyu, C. Zhao, D. Xiao, J. Zhu and S. J. Pennycook, *J. Am. Chem. Soc.*, 2019, **141**, 13987-13994.
8 W. Feng, B. Luo, S. Bian, E. Tian, Z. Zhang, A. Kursumovic, J. L. MacManus-Driscoll, X. Wang and L. Li, *Nat. Commun.*, 2022, **13**, 5086.
9 Y. Yang, Y. Ji, M. Fang, Z. Zhou, L. Zhang and X. Ren, *Phys. Rev. Lett.*, 2019, **123**, 137601.
10 F. Zhuo, H. Qiao, J. Zhu, S. Wang, Y. Bai, X. Mao and H. H. Wu, *Chin. Chem. Lett.*, 2021, **32**, 2097-2107.
11 H. Takenaka, I. Grinberg, S. Liu and A. M. Rappe, *Nature*, 2017, **546**, 391-395.
12 F. Li, S. Zhang, D. Damjanovic, L. Q. Chen and T. R. Shrout, *Adv. Funct. Mater.*, 2018, **28**, 1801504.
13 A. Kumar, J. N. Baker, P. C. Bowes, M. J. Cabral, S. Zhang, E. C. Dickey, D. L. Irving and J. M. LeBeau, *Nat. Mater.*, 2021, **20**, 62-67.
14 M. Eremenko, V. Krayzman, A. Bosak, H. Y. Playford, K. W. Chapman, J. C. Woicik, B. Ravel and I. Levin, *Nat. Commun.*, 2019, **10**, 2728.
15 H. Liu, X. Shi, Y. Yao, H. Luo, Q. Li, H. Huang, H. Qi, Y. Zhang, Y. Ren, S. D. Kelly, K. Roleder, J. C. Neuefeind, L. Q. Chen, X. Xing and J. Chen, *Nat. Commun.*, 2023, **14**, 1007.
16 R. A. Cowley, S. N. Gvasaliya, S. G. Lushnikov, B. Roessli and G. M. Rotaru, *Adv. Phys.*, 2011, **60**, 229-327.
17 M. J. Krogstad, P. M. Gehring, S. Rosenkranz, R. Osborn, F. Ye, Y. Liu, J. P. C. Ruff, W. Chen, J. M. Wozniak, H. Luo, O. Chmaissem, Z. G. Ye and D. Phelan, *Nat. Mater.*, 2018, **17**, 718-724.
18 N. Setter and L. E. Cross, *J. Mater. Sci.*, 1980, **15**, 2478-2482.
19 A. A. Bokov and Z. G. Ye, *J. Adv. Dielectr.*, 2012, **02**, 1241010.
20 D. Fu, H. Taniguchi, M. Itoh, S. y. Koshihara, N. Yamamoto and S. Mori, *Phys. Rev. Lett.*, 2009, **103**, 207601.
21 A. A. Bokov and Z. G. Ye, *J. Mater. Sci.*, 2006, 41, 31-52.
22 V. Westphal, W. Kleemann and M. D. Glinchuk, *Phys. Rev. Lett.*, 1992, 68, 847-850.
23 D. Phelan, C. Stock, J. A. Rodriguez-Rivera, S. Chi, J. Leão, X. Long, Y. Xie, A. A. Bokov, Z.-G. Ye, P. Ganesh and P. M. Gehring, *Proc. Natl. Acad. Sci. U.S.A.*, 2014, **111**, 1754-1759.
24 J. Wu, D. Xiao and J. Zhu, *Chem. Rev.*, 2015, **115**, 2559-2595.
25 Z. Sun, J. Zhang, H. Luo, Y. Yao, N. Wang, L. Chen, T. Li, C. Hu, H. Qi, S. Deng, L. C. Gallington, Y. Zhang, J. C. Neuefeind, H. Liu and J. Chen, *J. Am. Chem. Soc.*, 2023, **145**, 6194-6202.
26 L. Wang, H. Qi, S. Deng, L. Cao, H. Liu, S. Hu and J. Chen, *InfoMat*, 2023, **5**, e12362.
27 D. A. Keen, *Crystallogr. Rev.*, 2020, **26**, 143-201.
28 I. K. Jeong, T. W. Darling, J. K. Lee, T. Proffen, R. H. Heffner, J. S. Park, K. S. Hong, W. Dmowski and T. Egami, *Phys. Rev. Lett.*, 2005, **94**, 147602.
29 N. Zhang, H. Yokota, A. M. Glazer, Z. Ren, D. A. Keen, D. S. Keeble, P. A. Thomas and Z. G. Ye, *Nat. Commun.*, 2014, **5**, 5231.
30 M. S. Senn, D. A. Keen, T. C. A. Lucas, J. A. Hriljac and A. L. Goodwin, *Phys. Rev. Lett.*, 2016, **116**, 207602.
31 B. Jiang, T. Grande and S. M. Selbach, *Chem. Mater.*, 2017, **29**, 4244-4252.
32 M. G. Tucker, D. A. Keen, M. T. Dove, A. L. Goodwin and Q. Hui, *J. Phys. Condens. Matter*, 2007, **19**, 335218.
33 H. Liu, Z. Sun, S. Sun, Y. Zhang, H. Luo, H. Qi, L. Liu, J. C. Neuefeind, X. Xing and J. Chen, *Chem. Mater.*, 2022, **34**, 3985-3992.
34 M. Acosta, N. Novak, V. Rojas, S. Patel, R. Vaish, J. Koruza, G. A. Rossetti, Jr. and J. Rödel, *Appl. Phys. Rev.*, 2017, **4**, 041305.
35 Q. Hu and X. Wei, *J. Adv. Dielectr.*, 2019, **09**, 1930002.
36 Y. Huang, C. Zhao, B. Wu and J. Wu, *ACS Appl. Mater. Interfaces*, 2020, **12**, 23885-23895.
37 A. E. Glazounov, A. K. Tagantsev and A. J. Bell, *Phys. Rev. B*, 1996, **53**, 11281-11284.